

Spin filtering due to quantum interference in periodic mesoscopic networks

Amnon Aharony,¹ Ora Entin-Wohlman,¹ Yasuhiro Tokura,² and Shingo Katsumoto³

¹*Department of Physics and the Ilse Katz Center for Meso- and Nano-Scale Science and Technology, Ben Gurion University, Beer Sheva 84105, Israel*

²*NTT Basic Research Laboratories, NTT Corporation, Atsugi-shi, Kamagawa 243-0198, Japan*

³*Institute of Solid State Physics, University of Tokyo, Kashiwa, Chiba 277-8581, Japan*

(Dated: September 16, 2021)

We present several new results, extending our recent proposal of a spin filter based on a tight-binding model for a periodic chain of diamond-like loops [Phys. Rev. B **78**, 125328 (2008)]. In this filter, the Rashba spin-orbit interaction (which can be tuned by a perpendicular gate voltage) and the Aharonov-Bohm flux (due to a perpendicular magnetic field) combine to select only one propagating ballistic mode. For this mode, the electronic spins are fully polarized along a direction that can be controlled by the electric and magnetic fields and by the electron energy. All the other modes are evanescent. Generalizing the square diamonds into rhombi with arbitrary opening angles, we find that increasing these angles widens the parameter range for efficient filtering. A different gate voltage on the two sides of each rhombus is found to delocalize the electrons for energies on one side of the band center. We also compare our tight-binding model with models which use continuous quantum networks of one-dimensional wires, and find coincidence only when one chooses particular site energies at the nodes of the network.

PACS numbers:

I. INTRODUCTION

Future device technology and quantum information processing may be based on spintronics¹, where one manipulates the electron's spin (and not only its charge). Here we address attempts to build mesoscopic spin filters (or spin valves), which generate a tunable spin-polarized current out of unpolarized electron sources. Much recent effort in this direction uses narrow-gap semiconductor heterostructures, where the spins are subject to the Rashba² spin-orbit interaction (SOI): in a two-dimensional electron gas confined by an asymmetric potential well, the strength of this SOI can be varied by an electric field perpendicular to the plane in which the electrons move³. An early proposal of a spin field-effect transistor⁴ used the Rashba SOI to control the spin precession of electrons moving in quasi-one-dimensional wires.

Some of the most striking quantum effects arise due to interference, which is best demonstrated in quantum networks containing loops. Indeed, interference due to the Rashba SOI has been measured on a nanolithographically-defined square loop array⁵. Recently, several theoretical groups proposed spin filters based on a *single* loop, subject to both an electric and a magnetic (Aharonov-Bohm (AB))⁶ perpendicular fields (e.g Refs.^{7,8,9,10}). However, such devices produce a full polarization of the outgoing electrons only for *special values* of the two fields. Later work considered the effects of the Rashba SOI on the conductance of chains of loops. These included studies of chains of diamond-like loops^{11,12}, and studies of finite chains of circular loops¹³. Although both studies showed some destructive interference due to the SOI, they did not concentrate on the tuning of the fully polarized spins which can be obtained

in certain parameter ranges.

Recently¹⁴, we proposed a spin filter based on a periodic chain of diamond-like square loops, connected to each other at opposite corners [see Fig. 1]. Unlike the above earlier papers, which used a continuum description for the wires on the network, we used a simple tight-binding model, with quantum dots (or 'atoms') only at the nodes of the square diamonds. This allowed us to obtain transparent analytical expressions for the ballistic conductance through the chain and for the outgoing spin polarization. We found that a combination of both the Rashba SOI and the AB flux through each loop can result in destructive interference, which can block the transmission of all the spin components except one, which is then polarized at a tunable direction. Technically, this single spin direction is associated with a single propagating wave solution of the Schrödinger equation, while all the other solutions involve evanescent modes.

Here we extend our analysis of this diamond-like chain in several directions. First, we replace the previous square loops by rhombi, with a general angle 2β (Fig. 1). It turns out that the filter is more efficient for $\beta > \pi/4$. Second, we generalize our previous study, by allowing different site energies (controlled by appropriate gate voltages) on the various sites in the unit cell (i.e. sites a , b and c in Fig. 1). Different site energies at sites b and c turn out to have drastic effects on the ballistic conductance. Third, we propose using this filter at fixed electric and magnetic fields, controlling the outgoing polarization using a gate voltage. (In Ref.¹⁴ we worked at fixed energy, and varied the magnetic and electric fields.) Fourth, we replace each edge of each rhombus by a tight-binding chain of 'atoms' (or quantum dots). In this context, we compare our tight-binding approach with the continuous quantum network approach used in earlier work on the

same geometry^{11,12}. As we discuss elsewhere¹⁵, the two approaches are not equivalent.

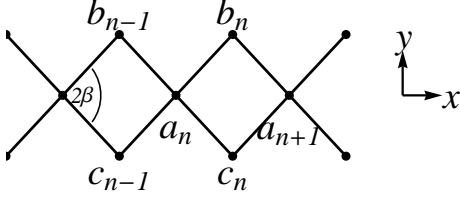


FIG. 1: Chain of diamonds.

Section 2 outlines the tight-binding model which we use for solving the Schrödinger equation on the periodic chain of generalized diamonds. Section 3 presents results for the polarization of the electrons in the regions where they are fully polarized. We compare our tight-binding approach to earlier continuum network models in Sec. 4, and summarize our results in Sec. 5.

II. GENERALIZED TIGHT-BINDING MODEL

The basic theory was presented in Ref.¹⁴. However, for the generalizations introduced here we find it easier to use the (rotated) coordinate axes shown in Fig. 1. Setting the opening angle of each diamond to 2β , the coordinates of the sites in the n 'th unit cell become $\mathbf{r}(a_n) = (n\bar{L}, 0, 0)$, $\mathbf{r}(b_n) = \mathbf{r}(a_n) + (L \cos \beta, L \sin \beta, 0)$ and $\mathbf{r}(c_n) = \mathbf{r}(a_n) + (L \cos \beta, -L \sin \beta, 0)$, where $\bar{L} = 2L \cos(\beta)$ is the basic step along the x -axis. We start with the simplest tight-binding model, which has 'atomic' sites only at the corners of the diamonds (this will be extended below). The hopping 2×2 unitary matrices within the n 'th diamond thus become

$$\begin{aligned} U_{ab}(n) &= e^{in\phi/2 + i\alpha\sigma_1}, & U_{ac}(n) &= e^{-in\phi/2 - i\alpha\sigma_2}, \\ U_{ba'}(n) &= e^{-i(n+1)\phi/2 - i\alpha\sigma_2}, \\ U_{ca'}(n) &= e^{i(n+1)\phi/2 + i\alpha\sigma_1}, \end{aligned} \quad (1)$$

where a' denotes the site a_{n+1} , $\boldsymbol{\sigma}$ is the vector of Pauli matrices, $\alpha = k_{SO}L$ (k_{SO} represents the strength of the Rashba term), $\sigma_1 = \sigma_x \sin \beta - \sigma_y \cos \beta$, $\sigma_2 = \sigma_x \sin \beta + \sigma_y \cos \beta$ and $\phi/(2\pi) = BL^2 \sin(2\beta)/\Phi_0$ is the number of flux units through each diamond. For each bond, the hopping matrix must be multiplied by the hopping energy, $J_{uv} = J$ (below we measure all energies in units of J).

Within the n 'th diamond, the Schrödinger equations for the spinors $\psi_a(n)$, $\psi_b(n)$ and $\psi_c(n)$ are

$$\begin{aligned} (\epsilon - \epsilon_a)\psi_a(n) &= -J(U_{ab}(n)\psi_b(n) + U_{ac}(n)\psi_c(n) \\ &+ U_{ba'}^\dagger(n-1)\psi_b(n-1) + U_{ca'}^\dagger(n-1)\psi_c(n-1)), \\ (\epsilon - \epsilon_b)\psi_b(n) &= -J(U_{ab}^\dagger(n)\psi_a(n) + U_{ba'}(n)\psi_a(n+1)), \\ (\epsilon - \epsilon_c)\psi_c(n) &= -J(U_{ac}^\dagger(n)\psi_a(n) + U_{ca'}(n)\psi_a(n+1)). \end{aligned} \quad (2)$$

Except for the special energies $\epsilon = \epsilon_b$, ϵ_c , which represent dispersionless solutions (not shown in the figures), we express $\psi_b(n)$ and $\psi_c(n)$ in terms of $\psi_a(n)$ and $\psi_a(n+1)$, and substitute into the equations for $\psi_a(n)$. We end up with effective one-dimensional equations,

$$4\lambda\Psi_a(n) = \mathbf{W}^\dagger\Psi_a(n-1) + \mathbf{W}\Psi_a(n+1), \quad (3)$$

with $4\lambda = \epsilon - \epsilon_a - 2\gamma_b - 2\gamma_c$, $\gamma_j = J^2/(\epsilon - \epsilon_j)$, $j = b, c$, and with the non-unitary 2×2 matrix

$$\begin{aligned} \mathbf{W} &= \gamma_b U_{ab}(n)U_{ba'}(n) + \gamma_c U_{ac}(n)U_{ca'}(n) \\ &\equiv 2(d - ib_y\sigma_y - b_z\sigma_z); & 2d &= a_+[c^2 - s^2 \cos(2\beta)], \\ 2b_y &= 2a_+cs \cos \beta, & 2b_z &= -ia_-s^2 \sin(2\beta), \end{aligned} \quad (4)$$

with $c = \cos \alpha$, $s = \sin \alpha$ and $a_\pm = \gamma_b e^{-i\phi/2} \pm \gamma_c e^{i\phi/2}$.

Assuming a propagating wave, $\Psi_a(n) = C e^{iq\bar{L}n} \chi(q)$, where $\chi(q)$ is a normalized spinor, we find that this spinor must obey $H\chi = \lambda\chi$, with

$$H = (e^{-iq\bar{L}}\mathbf{W}^\dagger + e^{iq\bar{L}}\mathbf{W})/4 \equiv (A + \mathbf{B} \cdot \boldsymbol{\sigma}), \quad (5)$$

where $A = \cos(q\bar{L})\Re d - \sin(q\bar{L})\Im d$, $B_x = 0$, $B_y = \cos(q\bar{L})\Im b_y + \sin(q\bar{L})\Re b_y$, and $B_z = \sin(q\bar{L})\Im b_z - \cos(q\bar{L})\Re b_z$. Therefore, χ is an eigenstate of $\mathbf{n} \cdot \boldsymbol{\sigma}$, with the unit vector $\mathbf{n} = \mathbf{B}/|\mathbf{B}|$: $\mathbf{n} \cdot \boldsymbol{\sigma} \chi_\mu = \mu \chi_\mu$, $\mu = \pm 1$, and we have $\lambda = A + \mu|\mathbf{B}|$. Thus, ϵ and q must obey the equation $(\lambda - A)^2 = B_y^2 + B_z^2$. At fixed q , this is a polynomial of degree 6 in ϵ , so that one expects 6 energy bands. In the special symmetric case where $\epsilon_b = \epsilon_c$, partially treated in Ref.¹⁴, two of these solutions represent dispersionless solutions at $\epsilon = \epsilon_b$, and thus one is left with only four bands (whose shape and location varies with ϵ_b). The value of ϵ_a only represents a shift in energy, so we fix $\epsilon_a = 0$. For $\epsilon_b > \epsilon_c = 0$ the dispersionless modes become dispersive, and in general the spectrum also becomes asymmetric with respect to $q \leftrightarrow -q$ and to $\epsilon \leftrightarrow -\epsilon$. An example of this phenomenon is shown in Fig. 2, for the square diamond ($\beta = \pi/4$).

As explained in¹⁴, the ballistic conductance at a given energy ϵ is equal to $G = (e^2/h)g$, where g is the number of propagating wave solutions which move in one direction. To study g , we now fix ϵ and solve the spectrum equation for q . In the general case, this equation turns into a quartic equation in $\cos(q\bar{L})$. This equation reduces to a quadratic equation for $\epsilon_b = \epsilon_c$. Out of the solutions for q we count only the right-moving propagating modes, with real q and with a positive velocity $v = \partial\epsilon/\partial q$. As in¹⁴, we again find ranges of ϵ with $g = 0, 1$ or 2 . Generally g depends on all three parameters ϵ , α and ϕ . Unlike Ref.¹⁴, where we fixed ϵ and presented results as functions of α or ϕ , here we fix ϕ and Fig. 3 presents contour plots of $g(\epsilon, \alpha/\pi)$ at $\phi = \pi/2$. As already indicated by Fig. 2, changing ϵ_b can open the large gap which existed in the symmetric case near $\epsilon = 0$. This can be seen by comparing the top two plots in Fig. 3: the right hand side plot, for $\epsilon_b = J$ and $\epsilon_c = 0$, is asymmetric with respect to changing the sign of ϵ , and it exhibits non-zero ballistic conductance at small positive energy. The

gate voltage governing ϵ_b can thus be used efficiently to vary the ballistic conductance between zero and non-zero values.

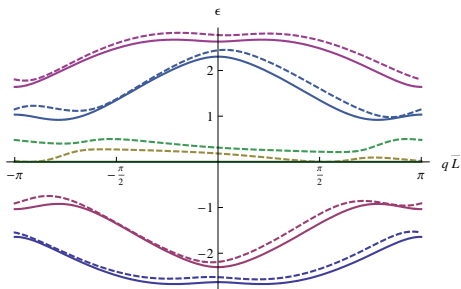


FIG. 2: Spectra for $\beta = \pi/4$, $\phi = .4\pi$, $\alpha = .2\pi$. Four full lines: $\epsilon_b = \epsilon_c = 0$. Six dashed lines: $\epsilon_b = .5$, $\epsilon_c = 0$. All energies are in units of J .

III. SPIN FILTER

In the regions with $g = 1$ we have only one propagating mode. As explained above, each mode is associated with a single spinor $\chi(q)$. The spinor of an electron coming from the left will in principle be written as a linear combination of all the four (or six) solutions. However, when $g = 1$ all the right moving modes except one are evanescent, i.e. they decay with distance. Therefore, the regions with $g = 1$ represent full polarization of the conducting electrons. For the symmetric case, Fig. 3 also compares between three values of the rhombus angle β . Interestingly, the square diamond ($\beta = \pi/4$) is not the optimal filter; increasing β broadens the regions with $g = 1$, where we have full polarization of the electrons. Therefore, we present below results for $\beta = .35\pi$.

FIG. 3: (Supplied separately) Contour plots in the $\epsilon - \alpha/\pi$ plane of the ballistic conductance g . (a) $\beta = \pi/4$ and $\epsilon_b = 0$, (b) $\beta = \pi/4$ and $\epsilon_b = J$. (c) $\epsilon_b = 0$ and $\beta = .15\pi$. (d) $\epsilon_b = 0$ and $\beta = .35\pi$. All other site energies are zero, and all plots have $\phi = \pi/2$. The values $g = 0, 1$ and 2 are represented by dark, medium and bright areas.

Looking at each panel in Fig. 3, we can identify cuts for which there are broad regions with $g = 1$. For each cut, the spin polarization is given by $\langle \chi | \boldsymbol{\sigma} | \chi \rangle = \mu \mathbf{n}$. Figure 4 shows these spin components, as a function of ϵ at fixed $\alpha = .45\pi$ (the spins are fully aligned in the z -direction for $\alpha = .5\pi$) and as a function of α at fixed $\epsilon = -1.1J$. As one can see, small changes in ϵ (determined by the Fermi energy) or in α (determined by the voltage which fixes the strength of the Rashba SOI) can cause jumps in S_y between large positive and negative values.

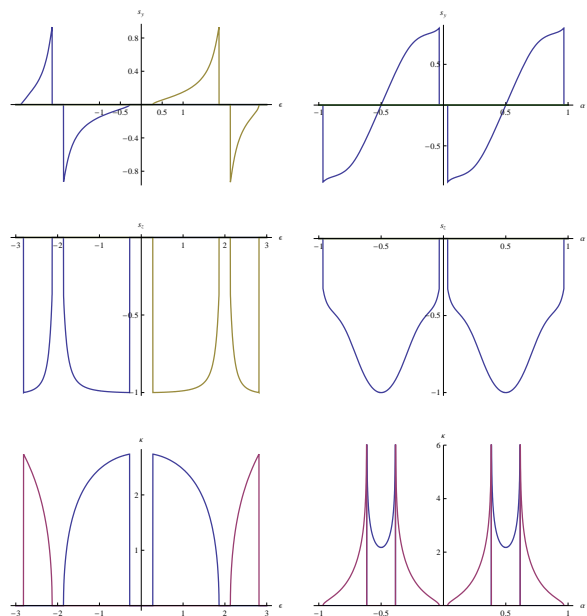


FIG. 4: Spin components S_y and S_z of the polarized propagating mode and the evanescent inverse decay length (in units of $1/\bar{L}$) versus ϵ at $\alpha = .45\pi$ (left) and versus α/π at $\epsilon = -1.1J$ (right). All plots have $\beta = .35\pi$. Data are shown only in regions where $g = 1$.

In practical situations, one will not use an infinite chain of diamonds. As discussed in Ref.¹⁴, the spin polarization is maintained even for a finite chain, provided we use adiabatic contacts at the exit. However, this finite chain must be long enough so that the evanescent modes will decay before the electrons come out. In the symmetric case, $\cos(q\bar{L})$ is found from solving the quadratic equation $(\lambda - A)^2 = |\mathbf{B}|^2$. For $g = 1$, one of the solutions has $|\cos(q\bar{L})| \leq 1$, and therefore a real q , while the other solution has $|\cos(q\bar{L})| > 1$, and therefore an imaginary $q = i\kappa$. The bottom panels in Fig. 4 show the imaginary part of q for these other modes, denoted by κ . As one can see, there are broad regions in which $\kappa > 1$, so that a small number of diamonds suffices for the evanescent modes to decay. Interestingly, κ diverges to infinity as α approaches special values, for which the coefficient of $\cos^2(q\bar{L})$ in the above quadratic equation approaches zero. Writing this equation as $ax^2 + bx + c = 0$, the solutions for small a are $\cos(q\bar{L}) = x_1 \approx -b/c$ and $\cosh(\kappa\bar{L}) = x_2 \approx -b/a$. Clearly, κ diverges as a approaches zero. Using the specific relations which follow Eq. (5), we identify $a = d^2 + b_y^2 - b_z^2$. It is then easy to check that the condition $a = 0$ is equivalent to $\det \mathbf{W} = \det \mathbf{W}^\dagger = 0$. When this condition is obeyed, \mathbf{W} and \mathbf{W}^\dagger have a vanishing eigenvalue, which means that the corresponding eigenvector is completely blocked [see Eq. (3)]. Interestingly, Ref.¹³ found similar blocking for finite chains at special values of the parameters.

IV. TIGHT-BINDING VERSUS CONTINUUM MODELS

A. Tight-binding model with many sites

We now generalize our model, by replacing each edge of a diamond by M bonds in series. Consider a single ‘large’ bond, e.g. the bond ab in Fig. 1. Solving the appropriate one-dimensional tight-binding model along this bond, we find that the spinor on the site m , $\psi^{(ab)}(m)$ [$0 \leq m \leq M$, with $\psi^{(ab)}(m=0) \equiv \psi_a$ and $\psi^{(ab)}(M) \equiv \psi_b$], is given by

$$\begin{aligned} \psi^{(ab)}(m) &= \frac{\sin[ka(M-m)]}{\sin(kaM)} [U_{ab}^\dagger]^{m/M} \psi_a \\ &+ \frac{\sin(kam)}{\sin(kaM)} [U_{ab}]^{(M-m)/M} \psi_b, \end{aligned} \quad (6)$$

where U_{ab} is the same as in Eq. (1), $a = L/M$ is the new lattice constant, and k is the wave vector for the one-dimensional solution, related to the energy ϵ and to the new elementary hopping energy J via $\epsilon = -2J \cos(ka)$.

We next discuss a general node on the network, u . The tight-binding equation at this node is

$$(\epsilon - \epsilon_u) \psi_u = -J \sum_v [U_{uv}]^{1/M} \psi^{(uv)}(1), \quad (7)$$

where we assumed that all the ‘large’ bonds are equivalent to each other, having the same number M of internal bonds, the same lattice constant a and the same hopping energy J . Substituting Eq. (6) on the right hand side, it is straightforward to rewrite Eq. (7) as

$$E_u \psi_u = -J \sum_v U_{uv} \psi_v, \quad (8)$$

with¹⁵

$$\begin{aligned} E_u &= -J \left(N_u \cos(kaM) - (N_u - 2) \sin(kaM) \cot(ka) \right. \\ &\quad \left. + \epsilon_u \sin(kaM) / [J \sin(ka)] \right), \end{aligned} \quad (9)$$

where N_u is the number of bonds meeting at site u . The generalization to arbitrary bonds is obvious. Equations (8) look exactly like our tight-binding equations (2), provided we replace $\epsilon - \epsilon_u$ by E_u . Therefore, we might expect some similarities in the solutions.

The equation for $\psi_b(n)$ in (2) now has E_b on the left hand side, and therefore the dispersionless modes contain all the solutions of $E_b = 0$. With $\epsilon_b = 0$, this yields $\epsilon = -2J \cos(ka)$, $ka = (n + 1/2)\pi/M$. Except for these energies, we again eliminate the side site spinors, restricting ourselves to the symmetric case, $\epsilon_b = \epsilon_c$. In this case, we also have $\gamma_b = \gamma_c \equiv \gamma$. It is then convenient to separate the common factor γ from Eq. (4), and rewrite the generalized Eq. (3) in the form

$$4\Lambda \psi_a(n) = \tilde{\mathbf{W}}^\dagger \psi_a(n-1) + \tilde{\mathbf{W}} \psi_a(n+1), \quad (10)$$

with $\tilde{\mathbf{W}} \equiv \mathbf{W}/\gamma$, and with $4\Lambda = E_a/\gamma - 4$, where now $\gamma = J^2/E_b$. The symmetric cases which we described above are characterized by the same matrix $\tilde{\mathbf{W}}$. Since all the spin physics described above resulted only from the matrix \mathbf{W} , which does not depend on the energy ϵ , all of that discussion will remain unchanged. The only effect of adding the internal bonds on each ‘large’ bond appears in the new parameter Λ , which is now given by

$$\Lambda = E_a E_b / (4J^2) - 1. \quad (11)$$

As before, the spectrum is determined by

$$\Lambda = \tilde{A} \pm |\tilde{\mathbf{B}}|, \quad (12)$$

where $\tilde{A} = A/\gamma$ and $\tilde{\mathbf{B}} = \mathbf{B}/\gamma$. For each value of q , Eq. (12) determines two values for Λ , which are independent of M and of ϵ . We then solve each of these equations for all possible values of ka , and obtain the energies of the various bands via $\epsilon = -2J \cos(ka)$.

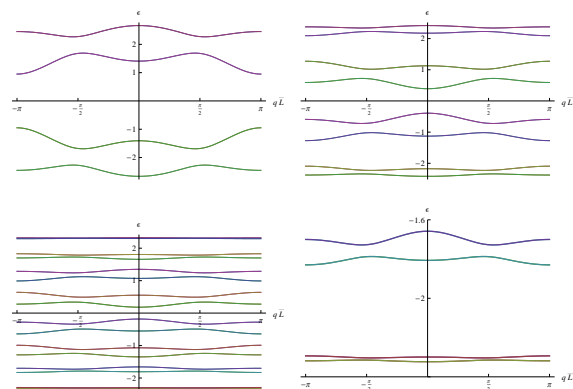


FIG. 5: Spectra for the diamond chain with M bonds on each ‘large’ bond, with $\beta = \pi/4$, $\phi = \pi/2$, $\alpha = .4\pi$. Top: $M = 1$ (left), $M = 2$ (right). Bottom: $M = 4$. All energies are in units of J .

For the special case $\epsilon_a = \epsilon_b = \epsilon_c = 0$, Eq. (11) reduces to $\Lambda = \cos(2kaM) - .5 \sin(2kaM) \cot(ka)$. Examples of the spectra for this case and for several values of M are shown in Fig. 5. Clearly, the number of bands increases with M . However, the basic qualitative shapes of $\epsilon(q)$ for all the bands are similar to each other. Thus, we expect that within each band we would reproduce the filtering properties described in Sec. 3. However, the energy scales for each band become narrower as M increases. This narrowing is most pronounced for the lowest band, which always appears below the band of the one-dimensional solutions, $\epsilon < -2J$. Within our tight-binding model, this narrow band involves an imaginary value of k , $\kappa = ik$, implying very small wave functions in the middle of each ‘large’ bond. This imaginary solution results from the solution of $\Lambda = \cosh(2\kappa aM) - .5 \sinh(2\kappa aM) \coth(\kappa a)$. At large M , Λ becomes negligible, and the two bands converge to a single band, with $\coth(\kappa a) \rightarrow 2$ and thus

$\epsilon = -2J \cosh(\kappa a) \approx -2.3094J$. The bottom panels in Fig. 5 show the spectrum for $M = 4$. The right hand side panel zooms on the two lowest bands, demonstrating that these bands maintain their qualitative features even as M increases. The lowest band does indeed narrow down, becoming dispersionless in the limit $M \rightarrow \infty$, where the equation $\Lambda = 0$ yields the solution $\epsilon = -2 \cosh(\kappa a)$, with $\coth(\kappa a) = 2$.

B. Continuum model

In contrast to our calculations, Refs.¹¹ and¹² used a continuum wire model for each ‘large’ bond on each diamond. Their solution for the spinor at distance x from node a on the bond ab is given by

$$\begin{aligned} \psi^{(ab)}(x) = & \frac{\sin[k(L-x)]}{\sin(kL)} [U_{ab}^\dagger]^{x/L} \psi_a \\ & + \frac{\sin(kx)}{\sin(kL)} [U_{ab}]^{(L-x)/L} \psi_b. \end{aligned} \quad (13)$$

Since the electron on each bond is now free, its energy is given by $\epsilon = \hbar^2 k^2 / (2m^*)$, and Bercieux *et al.* plot $\epsilon = k^2$. As usual with tight-binding equations, this solution coincides with our tight-binding solution (6) in the limit $M \rightarrow \infty$, keeping $a = L/M \rightarrow 0$ and $x = ma$. Having found these solutions, Refs.¹¹ and¹² proceed to use the Neumann boundary conditions at the nodes:

$$\sum_v \left. \frac{\partial \psi^{(uv)}(x)}{\partial x} \right|_{x=0} = 0. \quad (14)$$

With these conditions, they end up with equations like our (8), but with our E_u replaced by $-JN_u \cos(kL)$. Thus, they would have $\Lambda = \cos(2kL)$, and therefore $k = (n\pi \pm .5 \arccos \Lambda) / L$. These results, with $\epsilon = k^2 / 100$, are reproduced in the left panel of Fig. 6. Again, the qualitative shape of each band looks similar to ours. However, this approach cannot reproduce the lowest band with imaginary k which we found for finite M .

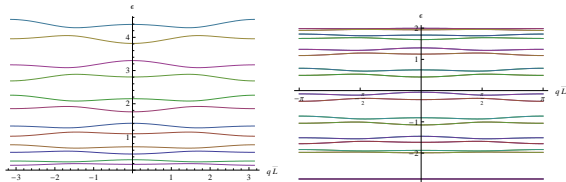


FIG. 6: Spectra for the diamond chain for the continuum model (left, with arbitrary energy units) and for the modified tight-binding ($M = 4$, $\epsilon_a = 2J$, right), with $\beta = \pi/4$, $\phi = \pi/2$, $\alpha = .4\pi$ and with energies in units of J .

As discuss in Ref.¹⁵, there is no way to make the tight-binding model and the continuum models identical for any finite M . However, in the limit $M \rightarrow \infty$ one can modify the tight-binding model, by setting a site energy $\epsilon_a = 2J$. With this special value, our Eq. (11) becomes $\Lambda = \cos(2kL) + \sin(2kL) \sin(ka)$, which becomes identical to the expression used in Refs.¹¹ and¹² when $a \rightarrow 0$. Unfortunately, we know of no good reason to choose this particular value for the site energy in the tight-binding model. The right hand panel in Fig. 6 shows results of the modified tight-binding model for $M = 4$. Except for the dispersionless band below the continuum, we expect these results to approach those in the left hand side panel as $M \rightarrow \infty$.

V. DISCUSSION

Reference¹⁴ already compared the results of a chain of diamonds to a single diamond. As also noted in Ref.¹³, having more loops in series broadens the parameter regions which yield full polarization. Reference¹⁴ also discussed the conditions for having full filtering on a chain of finite length. Here we have extended that discussion by showing that there exist broad regions with relatively short evanescent decay lengths, so that one can obtain filtering with relatively short chains.

In addition, we have shown that the filtering results are quite robust: in addition to the parameters discussed in Ref.¹⁴, the filtering persists upon changing many additional parameters (e.g. the opening angle of each diamond). We also mention the asymmetry of the spectra in the non-symmetric case, which implies that a large (positive or negative) bias voltage between the left and right hand ends of the device can yield different currents in the two directions.

We hope that the present discussion will stimulate attempts to realize our filter experimentally.

Acknowledgements. We acknowledge discussions with Joe Imry. AA and OEW acknowledge the hospitality of NTT and of the ISSP, where this project started, and support from the ISF and from the DIP.

¹ S. A. Wolf *et al.*, Science 294 (2001) 1488.

² E. I. Rashba, Fiz. Tverd. Tela (Leningrad) 2 (1960) 1224 [Sov. Phys. Solid State 2 (1960) 1109]; Y. A. Bychkov and E. I. Rashba, J. Phys. C 17 (1984) 6039.

³ T. Koga, J. Nitta, T. Akazaki, and H. Takayanagi, Phys. Rev. Lett. 89 (2002) 046801.

⁴ S. Datta and B. Das, Appl. Phys. Lett. 56 (1990) 665.

⁵ T. Koga, Y. Sekine, and J. Nitta, Phys. Rev. B 74 (2006) 041302.

⁶ Y. Aharonov and D. Bohm, Phys. Rev. 115 (1959) 485.

⁷ R. Citro, F. Romero and M. Marinaro, Phys. Rev. B 74 (2006) 115329.

- ⁸ B. Molnár, F. M. Peeters, and P. Vasilopoulos, Phys. Rev. B 69 (2004) 155335.
- ⁹ N. Hatano, R. Shirasaki, and H. Nakamura, Phys. Rev. A 75 (2007) 032107.
- ¹⁰ In fact, many of the results of Ref.⁹ were already found by Y. Oreg and O. Entin-Wohlman, Phys. Rev. B 46 (1992) 2393.
- ¹¹ D. Bercioux, M. Governale, V. Cataudella, and V. M. Ramaglia, Phys. Rev. Lett. 93 (2004) 056802.
- ¹² D. Bercioux, M. Governale, V. Cataudella, and V. M. Ramaglia, Phys. Rev. B 72 (2005) 075305.
- ¹³ B. Molnár, P. Vasilopoulos, and F. M. Peeters, Phys. Rev. B 72 (2005) 075330.
- ¹⁴ A. Aharony, O. Entin-Wohlman, Y. Tokura and S. Katsumoto, Phys. Rev. B 78 (2008) 125328.
- ¹⁵ A. Aharony and O. Entin-Wohlman, J. Phys. Chem. (in press); arXiv:0807.4088.

This figure "figure3a.png" is available in "png" format from:

<http://arxiv.org/ps/0812.2359v1>

This figure "figure3b.png" is available in "png" format from:

<http://arxiv.org/ps/0812.2359v1>

This figure "figure3c.png" is available in "png" format from:

<http://arxiv.org/ps/0812.2359v1>

This figure "figure3d.png" is available in "png" format from:

<http://arxiv.org/ps/0812.2359v1>